

# Bending rigidities and interdomain forces in membranes with coexisting lipid do- mains

Benjamin Kollmitzer,<sup>†,‡</sup> Peter Heftberger,<sup>†,‡</sup> Rudolf Podgornik<sup>§,¶,||</sup>,  
John F. Nagle<sup>\*\*</sup>, and Georg Pabst<sup>†,‡</sup> \*

<sup>†</sup> *University of Graz, Institute of Molecular Biosciences, Biophysics Division,  
NAWI Graz, Humboldstr. 50/III, A-8010 Graz, Austria.*

<sup>‡</sup> *BioTechMed-Graz, Austria.*

<sup>§</sup> *Department of Theoretical Physics, Jozef Stefan Institute, Ljubljana, Slovenia.*

<sup>¶</sup> *Department of Physics, Faculty of Mathematics and Physics, University of  
Ljubljana, Ljubljana, Slovenia.*

<sup>||</sup> *Department of Physics, University of Massachusetts, Amherst, Massachusetts,  
USA.*

<sup>\*\*</sup> *Department of Physics, Carnegie Mellon University, Pittsburgh, Pennsylvania,  
USA.*

\* Correspondence: georg.pabst@uni-graz.at

## Abstract

In order to precisely quantify the fundamental interactions between heterogeneous lipid membranes with coexisting liquid-ordered (Lo) and liquid-disordered (Ld) domains, we performed detailed osmotic stress SAXS experiments by exploiting the domain alignment in raft-mimicking lipid multibilayers. Performing a Monte Carlo (MC) based analysis allowed us to determine with high reliability the magnitude and functional dependence of interdomain forces concurrently with the bending elasticity moduli. In contrast to previous methodologies, this approach enabled us to consider the entropic undulation repulsions on a fundamental level, without having to take recourse to crudely justified mean-field like additivity assumptions. Our detailed Hamaker coefficient calculations indicated only small differences in the van der Waals attractions of coexisting Lo and Ld phases. In contrast, the repulsive hydration and undulation interactions differed significantly, with the latter dominating the overall repulsions in the Ld phase. Therefore, alignment of like domains in multibilayers appears to originate from both, hydration and undulation repulsions.

*Key words: osmotic stress experiments; interbilayer forces; liquid ordered phase; liquid disordered phase; membrane rafts; Monte Carlo simulations*

## **Introduction**

Diverse physiological processes in living systems depend on fundamental physical interactions between lipid membranes acting on the nanoscopic length scale. Of particular interest in this context are, besides intra-membrane interactions (1, 2), forces acting between membrane domains/rafts across the aqueous phase, which are also involved in their correlated mutual alignment. Such positional correlations are well established for liquid-ordered (Lo)/liquid-disordered (Ld) domains in model lipid multibilayers (3–11). Several groups have established compositional phase diagrams for mixtures of high-melting lipid, low-melting lipid and cholesterol, which exhibit Lo/Ld phase coexistence over a broad range of compositions and temperatures (12, 13). These systems mimic mammalian outer plasma membranes and enable studies of domain properties under well-defined conditions. Most recently, we reported structural details of Lo/Ld phases in two ternary lipid mixtures using a global small-angle X-ray scattering (SAXS) analysis for coexisting lipid domains (11). This analysis relies on the above mentioned mutual alignment of like domains. Domain-alignment is, however, also of biological relevance, for example in the context of, the immune response, where organization of receptor–ligand domains occurs during T-cell adhesion (14, 15). Both, the formation of such domains as well as the adhesion affinity depend strongly on thermal fluctuations and consequently on the bending rigidity of membranes (16, 17). It is therefore reasonable to expect that fundamental intermembrane interactions will play an important role also in receptor–ligand domain alignment.

Within the broad DLVO paradigm (18) the fundamental long-range interactions between soft material interfaces, mediated by their molecular environment,

such as solvation (hydration) interaction, electrostatic interaction, and van der Waals interaction, can be treated independently and additively. However, this additivity *Ansatz* is in general not vindicated for entropically driven bending undulation interactions that warrant a more sophisticated approach (18–20).

Besides the fundamental role of entropic membrane undulations, their relation with the membrane bending rigidity  $K_c$  (19), and through it their connection with diverse physiological processes, has spurred a sustained scientific interest (21). Shape analysis of giant unilamellar vesicles (GUV) (22), diffuse X-ray scattering from oriented lipid multibilayers (23), and GUV micropipette aspiration (24) are all techniques exploiting this connection, but none of them so far has been able to simultaneously determine the bending moduli for coexisting membrane phases. On the other hand, macroscopically sized domains form distinct lamellar lattices in multibilayer systems, enabling the application of *osmotic stress experiments* (8, 25). In such experiments, osmotic pressure is maintained by, e.g., large neutral polymers, such as poly-ethylene-glycol (PEG), which do not penetrate into the interbilayer water layer, while the corresponding bilayer separation and more recently also the specific line broadening due to fluctuations are measured by small-angle X-ray scattering (SAXS). Several groups, including ours, have previously applied this approach to study interactions between macromolecules, including lipid bilayers (8, 25–34).

The bare long-range DLVO interaction components, that couple macromolecular surfaces through their molecular environment, get inextricably intertwined through the thermally driven conformational fluctuations of the soft interfaces, making detailed predictions of the overall interaction nearly impossible. There-

fore, many studies in the past have resorted to describe such complicated thermal fluctuation effects by different mean-field/additivity approximations, where conformational fluctuation effects on the bare interaction potentials are included self-consistently (19, 20, 35–37). In contrast, additivity/mean-field approximations can be altogether avoided in the case of simulations that start from fundamental long-range DLVO interaction components and need no additional approximations to yield an accurate estimate for the total osmotic pressure in the system (38, 39).

In order to understand the coupling between bare interactions and thermal undulations in phase separated systems, we apply a gradient-based optimization algorithm to iteratively adjust the parameters entering MC simulations, i.e., the coefficients describing the strength and range of intermembrane interactions as well as the bending rigidity characterizing the thermal undulations, in order to best match simulation results with the experimental osmotic stress data for co-existing Lo/Ld phases. We demonstrate the capability of the simulation-driven analysis choosing a well-studied mixture of dioleoyl phosphatidylcholine (DOPC), distearoyl phosphatidylcholine (DSPC) and cholesterol (Chol) (40–42), previously shown to exhibit Lo/Ld domain alignment in the phase coexistence regime (11). We find that Lo domains are about three times more rigid than Ld domains, which exhibit significant contributions to domain repulsion from bending fluctuations. On the other hand, hydration forces decay much slower with domain separation between Lo domains. In turn, attractive van der Waals interactions were found to be of similar magnitude between Lo–Lo and between Ld–Ld domains. Our results provide insight into the strength and distance dependence of forces at play between like-domains as a prerequisite to devising theories for domain alignment.

## Materials and methods

### Sample preparation

DSPC, DOPC, and Chol were purchased from Avanti Polar Lipids, Inc., Alabaster, AL, USA and used without further purification. Poly(ethylene glycol) (PEG) with an average MW of 8000 was obtained from Fluka Chemie AG, Buchs, Switzerland and used as received.

After weighing, lipids were dissolved in chloroform/methanol 2:1 at concentrations of  $10 \text{ mg ml}^{-1}$  (43). We prepared the ternary lipid-only mixture DOPC/DSPC/Chol (0.42:0.37:0.21) in a glass vial and evaporated the organic solvent under a gentle nitrogen stream at  $30^\circ\text{C}$ . This lipid composition and its tie-line lie well inside the Lo/Ld phase coexistence region according to (40, 41), and the domains' structural properties have already been investigated with different methods (11, 42). Remaining solvent traces were removed by placing the samples in vacuum overnight.  $18 \text{ M}\Omega \text{ cm}^{-1}$  water (UHQ PS, USF Elga, Wycombe, UK) was added at  $20 \mu\text{l}$  water /mg lipid and the mixtures fully hydrated at  $50^\circ\text{C}$  for 4 hours with repeated freeze-thaw cycles.

To exert osmotic pressure on MLVs, samples were cooled to room temperature after hydration and aliquots overlaid with PEG dissolved in water, yielding final concentrations of 1–42 wt% PEG in water. Samples were protected against oxidation with argon, the vials closed and taped, and stored at  $4^\circ\text{C}$  for 7–10 days until the measurement. The osmotic equation of state for PEG, connecting its osmotic pressure with its solution concentration is well known (44) and allows for an accurate determination of the PEG osmotic pressure  $P$  by using previously reported

high resolution data (45).

## X-ray measurements

Small-angle X-ray scattering (SAXS) was performed at the Austrian SAXS beamline at ELETTRA, Trieste, Italy (46, 47), at a wavelength of 1.54 Å and an energy-dispersion  $\Delta E/E$  of  $2.5 \times 10^{-3}$ . A mar300 Image Plate 2D detector from marresearch, Norderstedt, Germany was used, covering a  $q$ -range from 0.2–7.1 Å<sup>-1</sup> and calibrated with silver-behenate (CH<sub>3</sub>(CH<sub>2</sub>)<sub>20</sub>–COOAg) with a  $d$ -spacing of 5.838 nm (48). Samples were filled into reusable quartz-glass capillaries and kept in a brass sample holder connected to a circulating water bath from Huber, Offenburg, Germany. The samples were equilibrated for 10 min at  $(20.0 \pm 0.1)$  °C before exposing them for 30 s to the X-ray beam.

The two dimensional detector signal was radially integrated with FIT2D (49, 50). Water background subtraction for samples without PEG was performed with Primus (51). For osmotically stressed samples however, additional scattering from PEG made a standard background subtraction impractical. Since the essential informations in this case were just the Bragg peaks' shapes and positions, we subtracted approximative backgrounds, obtained by interpolating between SAXS signals of pure water and PEG/water mixtures. Alternatively, one could just subtract an arbitrary smooth function from the measured data.

The reduced data were then fitted using a recently published, full  $q$ -range analysis method for coexisting liquid/liquid membrane domains (52). This method models each phase's contribution individually with a bilayer-structure and a superimposed membrane lattice. The lattice description is based on a modified Caillé

theory (53, 54) and therefore yields the average membrane periodicity  $d$  and the line shape parameter  $\eta$ , which is connected to the mean square fluctuation of the membrane spacing via  $\Delta^2 = \eta d^2 / \pi^2$  (32). The bilayer-structure of each phase is then modeled separately via probability distributions of quasi-molecular fragments (55).

Most importantly, the full  $q$ -range analysis allowed us to quantify the magnitude of fluctuations for coexisting domains. For both phases of stress-free samples, this also yields accurate electron density profiles, from which the bilayer thickness could be obtained; but this was not possible when osmotic pressure was applied. Instead, the osmotic thickening of  $d_B$  was calculated using  $d_B(P) = d_B(0) \cdot (K_A + P \cdot d(P)) / (K_A + P \cdot d_B(0))$  (31), where the area extension modulus  $K_A$  was estimated from published micropipette aspiration experiments on single lipids and binary lipid mixtures (56, 57), as detailed in Sec. S1 of the Supporting Material. The overall analysis was rather insensitive to uncertainties in  $K_A$  because the maximal change in bilayer thickness was only slightly larger than the uncertainty of the fit ( $\pm 2\%$ ). The definition of the bilayer thickness  $d_B$  was found to be more important. In principle one could determine optimal values of  $d_B$  via a joint fit with free MC parameters, but this problem is under-determined and led to bizarre values of  $d_B$  for different data sets (58). Instead, we defined  $d_B$  as the distance between the remotest lipid atoms (59), also known as the steric bilayer thickness (29); this yielded good fits and comparable results, while being directly accessible from the SAXS analysis.



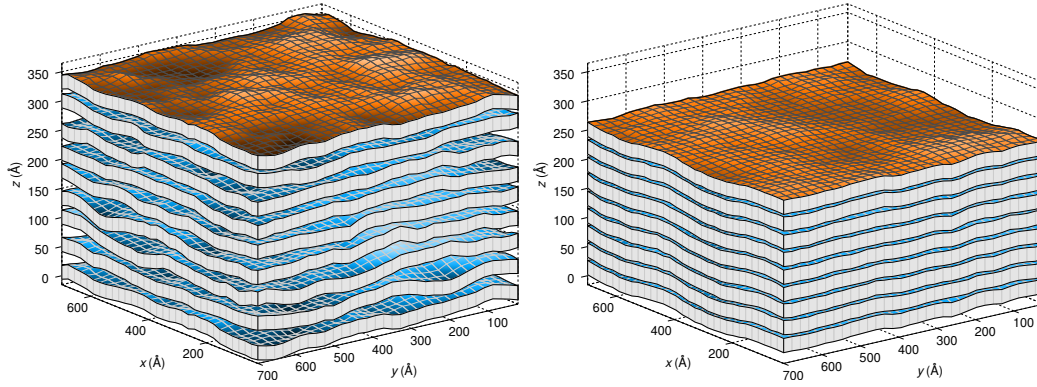


Figure 1: Real space snapshots of equilibrated Ld simulations at zero (left) and finite (5.5 MPa, right) osmotic pressure. Membranes are drawn with their average thickness. Deviations from the periodic lattice are color coded. Due to 3D periodic boundary conditions, the top-most (orange) and bottom-most (orange) membranes are equal. The most prominent effects of external pressure, a compression of the stack and a reduction of the fluctuations, are clearly visible.

## Membrane Monte-Carlo simulation

The simulation code used has been described previously in detail for a single membrane between two walls and for a stack of membranes (38, 39, 58). For completeness, but also to highlight our modifications, we briefly summarize its basic elements.

The system under consideration consists of a stack of  $M$  fluctuating and interacting membranes of size  $L \times L$ , as depicted in Fig. 1. The  $m$ -th membrane's displacement from its average plane is denoted as  $u_m(x, y)$ , the average distance between membranes  $\bar{a}$ , and the bending rigidity as  $K_c$ . Imposing periodic boundary conditions in all directions yields the Hamiltonian of a stack of membranes

$$\mathcal{H} = \sum_{m=0}^{M-1} \int \left( \frac{K_c}{2} (\nabla^2 u_m)^2 + \Phi(a_m) \right) dx dy, \quad (1)$$

where  $\Phi$  denotes the bare interaction potential, given here by the hydration repulsion and the van der Waals attraction, and  $a_m(x, y) = u_{m+1}(x, y) - u_m(x, y) + \bar{a}$  denotes the local distance between two membranes. We furthermore require  $a_m \geq 0$ , meaning that membranes cannot interpenetrate.

To reduce the system's degrees of freedom to a finite amount, the membranes are discretized on a square  $N \times N$  lattice. The simulation is performed in the constant pressure ensemble, (60) which converges for this model faster than constant volume simulations (39). Monte-Carlo updates are proposed in  $\bar{a}$  and in the complex coefficients  $u_m(q_x, q_y)$  of the Fourier transformation of  $u_m(x, y)$ . Simulating in Fourier space allows for larger moves, thereby accelerating equilibration (39). After every Monte Carlo step (MCS), which corresponds to degree of freedom  $(N^2M + 1)$  update proposals, we re-centered the coordinate system to correct for small center of mass movement as a new feature in the calculations.

Simulations were performed for  $L = 700 \text{ \AA}$ , several different  $N$  (6, 8, 12, 16, 24 and 32),  $M = 8$ , equilibration lengths of  $3 \times 10^3$  MCS, and collection lengths of  $10^4$  MCS, which typically exceeded the autocorrelation time by a factor of 100. Simulations were started with step sizes estimated from an approximative theory (20) and then subsequently optimized during equilibration, applying either dynamically optimized Monte Carlo (DOMC), or – as a new feature – the acceptance ratio method (ARM) as a backup if DOMC fails (58, 61).

Several observables can be determined from converged simulations, but the two most important quantities for comparison with SAXS experiments are the temporally- and spatially-averaged distance between membranes  $d_W = \langle \bar{a} \rangle$  and

the time average of its fluctuations

$$\Delta^2 = \overline{\langle (z_{m+1}(x, y) - z_m(x, y) - d_B - d_W)^2 \rangle}, \quad (2)$$

where the long bar denotes spatial averaging over  $(m, x, y)$ ,  $\langle \cdot \rangle$  denotes time averaging, and  $z_m(x, y) = u_m(x, y) + m \cdot (\bar{a} + d_B)$  is the  $m$ -th membrane's position in real-space. Specifically,  $d_W$  corresponds to the experimental thickness of the water layers separating the lipid bilayers, while  $\Delta$  is related to the experimental Caillé parameter  $\eta$  as detailed above.

It should be emphasized that our explicit purpose of making contact with the X-ray structure factor and the interactions between bilayers, requires much larger systems than can be presently envisioned either for all-atom simulations, used to obtain electron density profiles, or even for the most coarse grained molecular simulations (62). We require  $M$  bilayers in a stack, each bilayer having a large lateral size  $L$ . It has been shown in previous work (38), that  $L = 700 \text{ \AA}$  and  $M = 8$  are sufficient to obtain accuracies of 1% for  $d_W$  and  $\Delta$ , and that would require about 130 000 lipids with associated water in typical molecular simulations. Apart from simulation size, also the necessary timescales, which scale with the fourth power of the undulation wavelength (63, pp. 77–78), render molecular dynamics simulations for that purpose unfeasible. Furthermore, to fit the experimental data requires on the order of 100 separate simulations, distributed on multiple optimizations from different start points. In the membrane MC simulations we employ, each bilayer is reduced to a network consisting of  $N$  nodes in each of the two lateral directions and each node has only one degree of freedom. Computed observables change significantly with  $N/L$  (38, 39), so simulations were performed for a sequence of values

of  $N \in \{6, 8, 12, 16, 24, 32\}$  and then the observables were extrapolated towards  $N/L \rightarrow \infty$ . Further details of this finite size convergence are given in Sec. S2.

## Bare interaction potentials

For uncharged membranes, the potential at bilayer separation  $a$  is modeled canonically by (64)

$$\Phi(a) \simeq A\lambda \exp\left(-\frac{a}{\lambda}\right) - \frac{H}{12\pi a^2}. \quad (3)$$

The first term is the well-established empirical form of the solvent-mediated hydration interaction, which has been argued to originate from changes in various measures of order for the water structure at the membrane interface (65–67), with the strength  $A$  and the decay length  $\lambda$ , which is typically in the range of 1–2 Å (32). The second term describes the ubiquitous van der Waals interaction potential for two planar semi-infinite layers, with  $H$  being the Hamaker coefficient that in general also depends on the bilayer separation  $a$ ,  $H = H(a)$  (68, p. 15). This functional form is convenient because it can in fact describe both cases of either two finite-thickness layers interacting across a solvent layer (69), as well as effective pairwise interactions in an infinite stack of finite-thickness layers (70). For large solvent layer thickness the nonpairwise additive effects in the latter case become negligible and the van der Waals interaction potential for the two cases follows exactly the same separation dependence.

Due to the divergence of the van der Waals potential for  $a \rightarrow 0$ , the  $1/a^2$  term is cut off for  $a < 1 \text{ \AA}$  (38). In experiments, the collapse of charge neutral bilayers due to van der Waals forces is avoided by very short range steric interactions established by McIntosh et al. (71), but which occur at significantly higher osmotic pressures

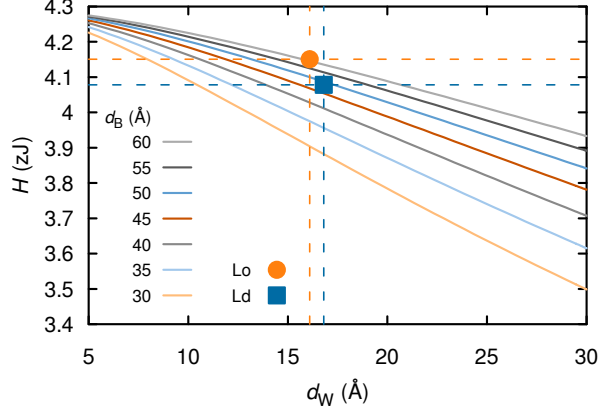


Figure 2: Hamaker coefficient  $H$  for hydrocarbon multilayers of height  $d_B$  and separation  $d_W$  in water. Highlighted are the applied values of  $H$  for Ld and Lo, which are described in the main text.

than those relevant for the present experiments, see also Fig. S5.

To calculate the Hamaker coefficient  $H$  *ab initio*, we had to approximate the lipid bilayers by pure hydrocarbon (72). Specifically, we calculated  $H$  for an infinite stack of hydrocarbon layers in water, based on a full multilayer Lifshitz formulation (70). The ranges for the hydrocarbon thicknesses  $d_B = 45 \text{ \AA}$  to  $60 \text{ \AA}$  and the water spacings  $d_W = 5 \text{ \AA}$  to  $30 \text{ \AA}$  were motivated by our experimental data. In this calculation range, differences in the Hamaker coefficient were within 10%. For our MC simulations the exact value of  $H$  matters most when all forces are of comparable magnitude, that is at vanishing external osmotic pressure. We therefore used the  $H$  values of  $4.08 \times 10^{-21} \text{ J} = 4.08 \text{ zJ}$  for Ld and  $4.15 \text{ zJ}$  for Lo domains, see Fig. 2.

Both components of the bare potential, i.e. hydration and van der Waals, cause

partial bare pressures between neighboring membranes given by (73)

$$P_{hyd}(d_W) = A \exp\left(-\frac{d_W}{\lambda}\right), \quad P_{vdW}(d_W) = -\frac{H}{6\pi d_W^3}. \quad (4)$$

For comparison to previous reports using mean-field/additivity approximations for modeling undulation interactions, one can obtain an effective decay constant  $\lambda_{und}$  by subtracting bare contributions from experimental data, i.e.  $P_{und} = P - P_{hyd} - P_{vdW}$  (39). The undulation decay constant then results from a fit of  $P_{und} = A_{und} \exp(-\lambda_{und}/d_W)$ , with the two adjustable parameters  $A_{und}$  and  $\lambda_{und}$ . Because the undulation pressure deviated significantly from a perfect exponential, we limited the fit to large separations ( $d_W \geq 14 \text{ \AA}$ ).

## Optimizing parameters against experimental data

Calculation of the Hamaker coefficient  $H$ , as described above, allowed us to reduce the number of free fitting parameters for the simulations to three,  $\vec{\Lambda} = (A, \lambda, K_c)$ , for a joint analysis of domain separation and fluctuation data (see below).

We implemented a least squares routine with Matlab<sup>®</sup> (74), utilizing its trust region reflective optimization algorithm to minimize the sum of the squared residues

$$\chi^2(\vec{\Lambda}) = \sum_i \left( \frac{d_{W,i} - d_W(P_i; \vec{\Lambda})}{U_{\text{eff}}(d_{W,i})} \right)^2 + \left( \frac{\Delta_i - \Delta(P_i; \vec{\Lambda})}{U_{\text{eff}}(\Delta_i)} \right)^2, \quad (5)$$

where  $d_{W,i}$  and  $\Delta_i$  are the experimentally determined values at fixed osmotic pressure  $P_i$ ,  $d_W(P_i; \vec{\Lambda})$  and  $\Delta(P_i; \vec{\Lambda})$  are simulation results, and  $U_{\text{eff}}(f)$  is the effective

uncertainty of a given quantity  $f$ , derived from

$$U_{\text{eff}}^2(f) = U^2(f_{\text{exp}}) + U^2(f_{\text{sim}}) + \left( \frac{\partial f_{\text{sim}}}{\partial P} \cdot U(P_i) \right)^2. \quad (6)$$

The agreement between model and data was evaluated by the reduced  $\chi_{red}^2 = \chi^2/\tilde{N}$ , where  $\tilde{N}$  equals the number of data points minus the number of free parameters (75, p. 268). The Jacobian for this gradient based algorithm and the derivative in Eq. (6) were computed with the histogram reweighting method described in Sec. S3. Once the iteration converged, the uncertainties of the fit parameters were determined from the curvature of  $\chi_{red}^2$ . In order to locate the global optimum, several iterations from randomly chosen initial parameter sets were performed.

To test our implementation, we fitted simulation results determined for one reasonable parameter set  $\vec{\Lambda}'$ , by starting the least squares from several different initial starting points  $\vec{\Lambda}$ . Within 3–5 iterations, these optimizations converged towards the correct values  $\vec{\Lambda}'$ , thereby indicating that the weighted histogram based differentiation and the fit were correctly implemented. For the experimental data sets, convergence was usually reached within 10 iterations. However, due to the stochastic nature of the simulations and the consequential randomness of results and derivatives, the optimization algorithm propagated poorly in flat regions, i.e. small  $\vec{\nabla}\chi_{red}^2$ . Because  $\chi_{red}^2(\vec{\Lambda})$  is a smooth function and its gradient has to vanish at extrema, the optimization algorithm's efficiency decreased, the closer it got to the optimum. This was another reason for starting several independent iterations (76).

As a further test case, we re-analyzed previously published osmotic pressure

data of pure dimyristoyl-phosphocholine (DMPC) bilayers (32), yielding very reasonable values and a good agreement between simulations and experiments. Details are given in Sec. S4. Thus, we conclude that our method provides a robust analysis for interactions in fluctuating membrane assemblies.

## Results and Discussion

### X-ray analysis

SAXS patterns were analyzed as detailed previously by a Caillé theory-based analysis (11). Figure 3 showcases the analysis for two samples at osmotic pressures of 34 kPa and 2.4 MPa, demonstrating that shapes and positions of Bragg reflections are well reproduced. Consistent with previous studies (8, 9, 11), we find sharper and more prominent Bragg reflections for the Lo phase due to its decreased bending fluctuations, compared to the coexisting Ld phase. Fits for all other samples are shown in Sec. S5. For increased osmotic pressures, Bragg peaks shifted towards higher  $q$  and became more prominent. This is due to the decrease of bilayer separation which goes in hand with a reduction of bending fluctuations in agreement with previous reports (32, 77).

Peak line-shapes for Lo and Ld domains were found to be well described by the applied Caillé theory, particular at low osmotic pressure (Fig. S4). Since this theory is incapable of fitting peaks from lamellar gel phases (78), we conclude that neither peaks assigned to the Lo, nor to the Ld phase can originate from a gel phase. This is also consistent with reported compositional DSPC/DOPC/Chol phase diagrams (40, 41) and a recent SAXS study from our lab, reporting for the



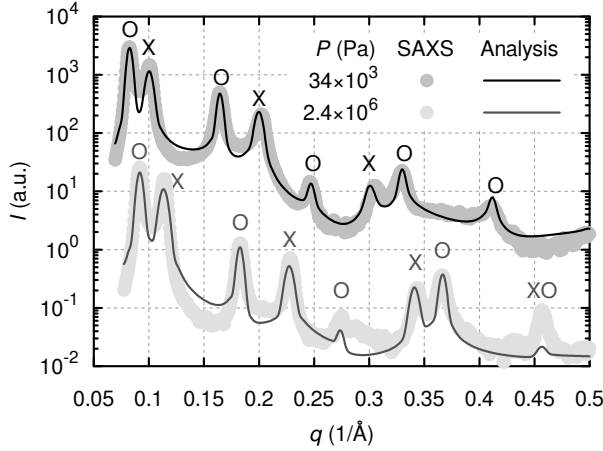


Figure 3: Calculated scattering intensities (solid lines) from full  $q$ -range analyses, compared with recorded SAXS data from coexisting phases (dots) for two different osmotic pressures  $P$ . Bragg reflections from aligned Lo and Ld domains are indicated by symbols O and X, respectively.

identical lipid mixture that the structural parameters match those of Lo and Ld phases at the tie-line endpoints (11).

Fit quality of SAXS spectra worsened for increased PEG concentrations, see Fig. 3 or Sec. S5. Probably the underlying Caillé theory loses its applicability for the increased order experienced at elevated osmotic pressures. While effects on domain separation were negligible, fluctuations determined from the fits became increasingly skewed with osmotic pressure, in particular for Lo domains (see below).

The effect of osmotic pressure on the lamellar repeat spacing  $d$ , as determined from the SAXS analysis, is plotted in Fig. 4. At high osmotic stress, the distance between bilayers is effectively set by the repulsive hydration interaction which dominates the repulsive fluctuation interaction and the attractive van der Waals

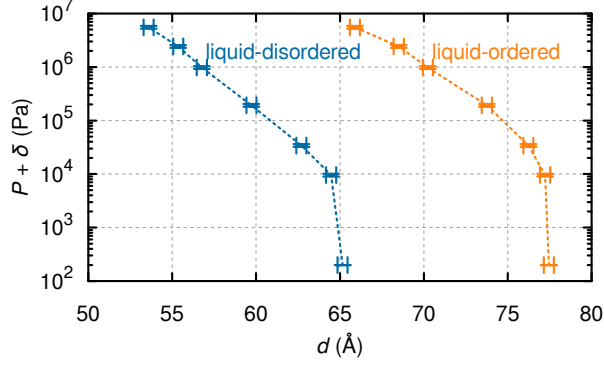


Figure 4: Osmotic pressure  $P$  vs membrane periodicity  $d$  for Ld and Lo determined by SAXS analysis (79). Dashed lines are meant solely as a guide for the eye.

interaction. As osmotic pressure is decreased, the water spacing between bilayers  $d_W$  increases and the fluctuation interaction eventually dominates the hydration interaction. As the osmotic pressure is reduced to zero, the attractive van der Waals force balances the total repulsive forces, resulting in finite  $d_W$  and  $d$  values.

Within experimental uncertainty, the two isotherms in Fig. 4 are rather similar when the difference in membrane thickness is taken into account ( $d_B^{Ld} = (48.5 \pm 1.0) \text{ \AA}$  and  $d_B^{Lo} = (61.3 \pm 1.2) \text{ \AA}$ ). Of course, identical isotherms would imply that all the interactions are identical. However, significant experimental differences were observed in the fluctuation behavior as detailed below, corroborating the crucial advantage of jointly analyzing fluctuations and osmotic pressure isotherms in order to obtain the interaction parameters (32).

Table 1: Optimal parameters determined for describing the coexisting Lo/Ld phases in DOPC/DSPC/Chol (0.42:0.37:0.21). Errors as obtained from the fitting routine, see text for further details.

	Ld	Lo
$K_c/zJ$	$44 \pm 10$	$120 \pm 20$
$A/\text{Pa}$	$10^{8.3 \pm 0.2}$	$10^{8.1 \pm 0.2}$
$\lambda/\text{\AA}$	$1.37 \pm 0.15$	$1.74 \pm 0.15$
$\chi_{red}^2$	$1.5 \pm 0.5$	$5.8 \pm 0.5$

## Optimized simulations

The experimental data and the results of optimized simulations are compared in Fig. 5, while Tab. 1 lists results for the interaction parameters. Experimental errors for  $d_W$  and  $\eta$  were obtained from the SAXS analysis and for  $P$  were estimated to equal the pipetting error of 6% for viscous PEG solutions. To quantify the agreement between data and simulations, we report  $\chi_{red}^2$ , which becomes ca. 1 if the differences are compatible with experimental errors (75, p. 268). This is the case for the Ld phase, where simulations and experimental data match ideally, but the mismatch for Lo is bigger than expected ( $\chi_{red}^2 = 6$ ).

We are inclined to attribute this discrepancy for Lo at least partially to the limited applicability of the Caillé theory for highly ordered systems, as described in the previous section. Indeed, deviations in  $\Delta$  are especially pronounced for small bilayer separations, i.e. at high osmotic pressures. In light of these discrepancies, we suggest that the experimental uncertainties determined for the Lo phase are rather too small because they do not take into account the decreasing applicability of the Caillé theory for more ordered phases whose fluctuations are suppressed by low hydration.

While differences in  $P(d_W)$  are insignificant between Ld and Lo (see also

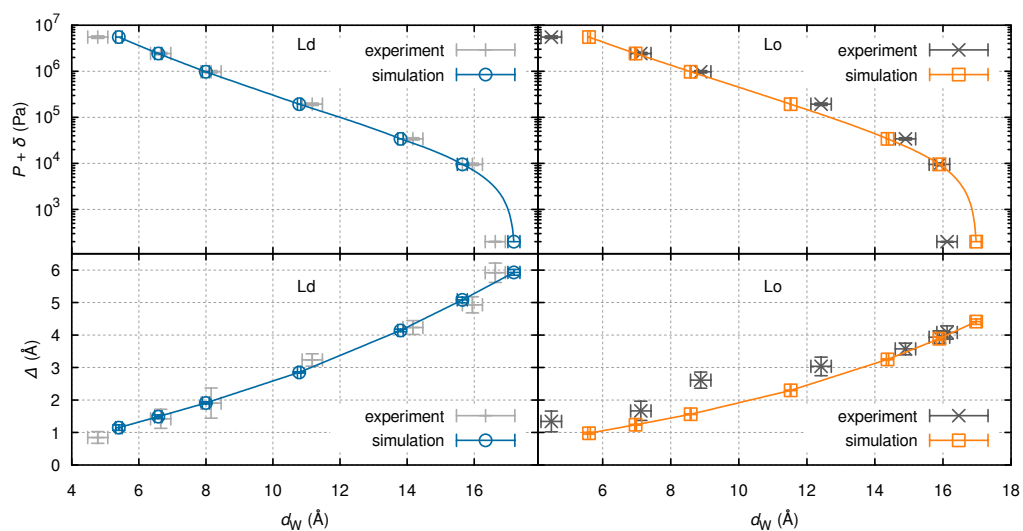


Figure 5: Osmotic pressure (top) and fluctuations (bottom) vs water-layer thickness for best fit of membrane MC simulation (cyan/orange) against SAXS data (gray) (79). Solid lines were obtained by exponentially interpolating fluctuation contributions.

Fig. 4), fluctuations of the Lo phase, containing most of the DSPC and about thrice as much cholesterol as Ld, are evidently smaller (Fig. 5). In the continuum mechanics treatment used in the simulations, this increase in bilayer stiffness is captured by a threefold higher  $K_c$  for Lo, see Tab. 1.

The values obtained by us for  $K_c$  compare well with previously reported results from different techniques. Bending rigidities of binary DOPC/cholesterol mixtures have been measured by several groups, ranging from  $(60 \pm 8)$  to  $(100 \pm 25)$  zJ and were found to be largely unchanged by the cholesterol content (80–83). This supports the  $K_c = (44 \pm 10)$  zJ obtained for Ld, where DOPC is the main constituent (41). In contrast, a larger concentration of saturated lipids, for which  $K_c$  does increase with cholesterol (80), is present in the Lo phase, so a larger bending rigidity would be expected for Lo than for Ld. Our finding of  $K_c = (120 \pm 20)$  zJ for the Lo phase is consistent with this expectation.

Furthermore, molecular dynamics (MD) simulation results are available for comparison. Khelashvili et al. (84) used the reported tie-line endpoint compositions (41) to separately simulate the liquid-disordered and -ordered phases, obtaining bending moduli of 80–130 zJ for Ld and 340–440 zJ for Lo. Although these values are large compared to our results, both methods find a strong increase of  $K_c$  between Ld and Lo.

In agreement with Ref. 85, we find that a rather simple model suffices to relate bending to area extension moduli for cholesterol-rich samples (86). Based on the assumption that the main contribution to membrane rigidity comes from the stiff cholesterol ring of size  $\delta'$ , Pan et al. used the relationship  $\delta'^2 = 12K_c/K_A$ . For our samples, with  $K_A = 430 \text{ mN m}^{-1}$  and  $2100 \text{ mN m}^{-1}$  (see Sec. S1 for details), this

equation yields  $\delta' = 11 \text{ \AA}$  and  $8 \text{ \AA}$  for Ld and Lo, respectively, in good agreement to actual cholesterol ring sizes of about  $9 \text{ \AA}$ , giving additional support to our analysis.

## Interdomain forces

As stated before, the differences between Ld and Lo in the  $P$  vs  $d_W$  data sets are small. However, a more thorough investigation of these quantities yields interesting insights. Because good fits to these data were obtained, the total pressure  $P$  is readily dissected into its individual contributions from the fundamental surface forces, whose functional dependences are plotted in Fig. 6.

The thicker Lo bilayer causes an increase in the Hamaker coefficient, but only by 3% compared to the Ld phase; this is a minor difference in the van der Waals interaction that is hardly noticeable in the  $P_{vdW}$  curve in Fig. 6. For small bilayer separations, the hydration interactions are of similar magnitude and represent, as expected, the dominant contribution to the total interaction potential for both phases. Despite these similarities, the fluctuation pressure starts to surpass the hydration pressure already at much smaller separations  $d_W$  for Ld than for Lo. This difference implies, in contrast to the ordered phase, that the undulation interaction becomes the most important repulsive interaction over a wider range of bilayer separations in the case of the disordered phase. Stronger repulsions due to fluctuation interactions are of course reasonable because thermal undulations were found to be significantly increased for the Ld phase (Fig. 5). Nevertheless, even in the Lo phase, the thermal undulation interaction dominates the hydration force over the most important, well hydrated range of  $d_W$ , starting at separations of  $12 \text{ \AA}$ .

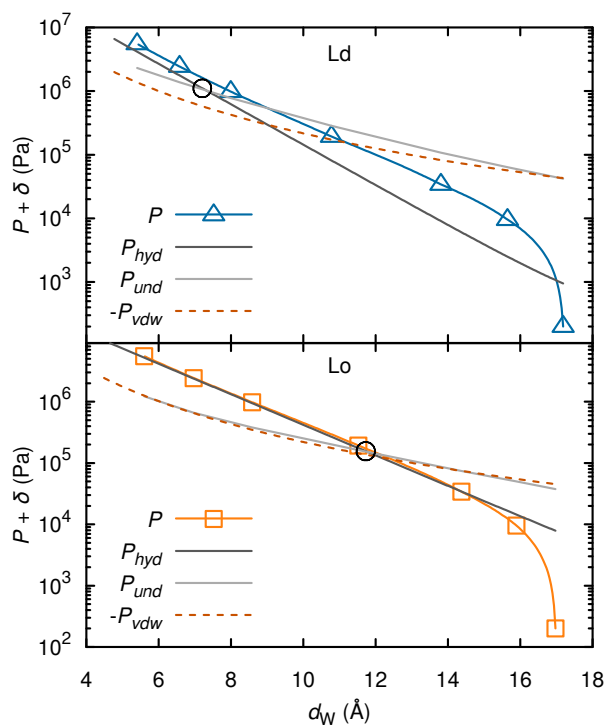


Figure 6: Partitioning of total pressure  $P$  into contributions from hydration  $P_{hyd}$ , van der Waals  $P_{vdw}$ , and undulations  $P_{und}$  for Ld (top) and Lo (bottom) (79). The large open black circles show the values of the separation  $d_W$ , at which hydration and undulation pressure are equal. Due to the additive constant  $\delta$ , the hydration pressure deviates from a straight line at low  $P$ .

We obtained almost exponentially decreasing fluctuation forces of the scaling form  $\propto \exp(-z/\lambda_{und})$ , with effective decay lengths  $\lambda_{und} \approx 3.3 \text{ \AA}$  and  $3.7 \text{ \AA}$  for Ld and Lo, respectively. The ratio of fluctuation to hydration decay length  $\lambda_{und}/\lambda$  is obtained as 2.4 for Ld and 2.1 for Lo. While the mean-field theory predicted its value as 2.0 (20), values of 2.4 have been reported for simulations (38, 39), and 2.0–3.0 from other experiments (8, 32, 33).

Compared to Lo, a significantly shorter decay length for the hydration interaction pressure was found for the Ld phase. At present, the origin for this difference is unclear. However, it is this difference combined with the larger fluctuation force that gives  $P$  versus  $d_W$  curves that are nearly the same for Lo and Ld, both with fully hydrated  $d_W$  close to  $17 \text{ \AA}$ .

Domain alignment across interlamellar aqueous phases has recently been hypothesized to be caused by water network mismatch due to the different hydration properties of Lo and Ld phases (3). In support of this postulation, we observed significantly different hydration forces and nearly equal van der Waals forces for both phases. Thermal fluctuations were however neglected in the aforementioned hypothesis, while we now find considerable differences specifically in the undulation forces for coexisting domains. Their importance is especially striking near full hydration, where undulation and van der Waals pressures surpass hydration repulsion by an order of magnitude (see Fig. 6).

## Conclusion

We have evaluated the fundamental long-range interactions between coexisting Lo and in Ld domains in DOPC/DSPC/cholesterol, which is a frequently used model



system for mammalian outer plasma membranes (11–13, 40–42, 87, 88). Because we could do this at concentrations where Lo and Ld domains coexist, we were able to avoid all uncertainties in the phase diagram and its associated tie-lines between Lo and Ld phases. This work combines methodology from three separate inputs: SAXS/osmotic stress experiments, comprehensive Monte Carlo simulations, and detailed calculations of van der Waals interactions.

The reported values for fundamental surface forces and bending moduli are the first of their kind being, directly obtained from coexisting Lo/Ld domains. The underlying full  $q$ -range SAXS analysis allowed us to quantify the extent of fluctuations and capture their dependence on osmotic pressure, which proved essential for determining the bending rigidities of cholesterol-rich phases. We obtained bending moduli of 44 zJ for Ld and a roughly threefold higher value for Lo domains, attributable to their larger concentrations of saturated lipid and cholesterol.

While we obtained almost identical van der Waals interactions for aligned Lo and Ld domains, the remaining interactions, however, turned out to be strikingly different: decay lengths of the hydration pressures differed by 25% between Lo and Ld phases, and repulsions due to thermal fluctuations were found to be significantly increased for Ld. These findings provide evidence that a combination of hydration repulsion and the fluctuation-driven undulation repulsion must be considered in any quantitative explanation of the long-range positional correlations between aligned Lo and Ld domains. In particular the strong entropic contribution from undulating Ld domains may be a leading term to be considered. We therefore expect that our study will form the base for a concise theory of domain alignment.

## **Author Contributions**

B.K. designed and performed research, analyzed data and wrote the paper; P.H. designed and performed research and analyzed data; R.P. and J.F.N. contributed analytic tools and wrote the paper; G.P. designed and performed research and wrote the paper.

## **Acknowledgments**

This work is supported by the Austrian Science Fund FWF, Project no. P24459-B20 to GP. The computational results presented have been achieved using the Vienna Scientific Cluster (VSC). The authors thank Alexander Rieder and Heinz Amenitsch for experimental support and Hans Gerd Evertz for critical review of the simulation and advice regarding finite size convergence. Support for the original development of the MC software was provided to JFN under grant GM44976 from the U.S. National Institutes of Health. RP would like to acknowledge the SLO-A bilateral grant N1-0019 of the Slovene Research Agency.

## **Supporting Citations**

References (94–103) appear in the Supporting Material.

## References

1. Semrau, S., T. Idema, T. Schmidt, and C. Storm, 2009. Membrane-Mediated Interactions Measured Using Membrane Domains. *Biophys. J.* 96:4906–4915.
2. Ursell, T. S., W. S. Klug, and R. Phillips, 2009. Morphology and interaction between lipid domains. *PNAS* 106:13301–13306.
3. Tayebi, L., Y. Ma, D. Vashaee, G. Chen, S. K. Sinha, and A. N. Parikh, 2012. Long-range interlayer alignment of intralayer domains in stacked lipid bilayers. *Nat. Mater.* 11:1074–1080.
4. Karmakar, S., and V. A. Raghunathan, 2005. Structure of phospholipid-cholesterol membranes: An x-ray diffraction study. *Phys. Rev. E* 71:061924.
5. Chen, L., Z. Yu, and P. J. Quinn, 2007. The partition of cholesterol between ordered and fluid bilayers of phosphatidylcholine: A synchrotron X-ray diffraction study. *Biochim. Biophys. Acta, Biomembr.* 1768:2873–2881.
6. Mills, T. T., S. Tristram-Nagle, F. A. Heberle, N. F. Morales, J. Zhao, J. Wu, G. E. S. Toombes, J. F. Nagle, and G. W. Feigenson, 2008. Liquid-Liquid Domains in Bilayers Detected by Wide Angle X-Ray Scattering. *Biophys. J.* 95:682–690.
7. Staneva, G., C. Chachaty, C. Wolf, K. Koumanov, and P. J. Quinn, 2008. The role of sphingomyelin in regulating phase coexistence in complex lipid model membranes: Competition between ceramide and cholesterol. *Biochim. Biophys. Acta, Biomembr.* 1778:2727–2739.

8. Pabst, G., B. Boulgaropoulos, E. Gander, B. R. Sarangi, H. Amenitsch, V. A. Raghunathan, and P. Laggner, 2009. Effect of Ceramide on Nonraft Proteins. *J. Membr. Biol.* 231:125–132.
9. Yuan, J., A. Kiss, Y. H. Pramudya, L. T. Nguyen, and L. S. Hirst, 2009. Solution synchrotron x-ray diffraction reveals structural details of lipid domains in ternary mixtures. *Phys. Rev. E* 79:031924.
10. Uppamoochikkal, P., S. Tristram-Nagle, and J. F. Nagle, 2010. Orientation of Tie-Lines in the Phase Diagram of DOPC/DPPC/Cholesterol Model Biomembranes. *Langmuir* 26:17363–17368.
11. Heftberger, P., B. Kollmitzer, A. A. Rieder, H. Amenitsch, and G. Pabst, 2015. In Situ Determination of Structure and Fluctuations of Coexisting Fluid Membrane Domains. *Biophys. J.* 108:854–862.
12. Heberle, F. A., and G. W. Feigenson, 2011. Phase Separation in Lipid Membranes. *Cold Spring Harb. Perspect. Biol.* 3:a004630.
13. Marsh, D., 2009. Cholesterol-induced fluid membrane domains: A compendium of lipid-raft ternary phase diagrams. *Biochim. Biophys. Acta, Biomembr.* 1788:2114–2123.
14. Monks, C. R. F., B. A. Freiberg, H. Kupfer, N. Sciaky, and A. Kupfer, 1998. Three-dimensional segregation of supramolecular activation clusters in T cells. *Nature* 395:82–86.
15. Grakoui, A., S. K. Bromley, C. Sumen, M. M. Davis, A. S. Shaw, P. M. Allen,

- and M. L. Dustin, 1999. The Immunological Synapse: A Molecular Machine Controlling T Cell Activation. *Science* 285:221–227.
16. Różycki, B., R. Lipowsky, and T. R. Weikl, 2010. Segregation of receptor–ligand complexes in cell adhesion zones: phase diagrams and the role of thermal membrane roughness. *New J. Phys.* 12:095003.
  17. Hu, J., R. Lipowsky, and T. R. Weikl, 2013. Binding constants of membrane-anchored receptors and ligands depend strongly on the nanoscale roughness of membranes. *PNAS* 110:15283–15288.
  18. Israelachvili, J. N., 2011. Interactions of Biological Membranes and Structures. *In* Intermolecular and surface forces, Academic Press, Burlington, MA, 577–616.
  19. Helfrich, W., 1978. Steric Interaction of Fluid Membranes in Multilayer Systems. *Z. Naturforsch., A: Phys. Sci.* 33:305.
  20. Podgornik, R., and V. A. Parsegian, 1992. Thermal-mechanical fluctuations of fluid membranes in confined geometries: the case of soft confinement. *Langmuir* 8:557–562.
  21. Pabst, G., 2013. Coupling Membrane Elasticity and Structure to Protein Function. *In* Advances in Planar Lipid Bilayers and Liposomes, Elsevier, volume 18, 81–109.
  22. Méléard, P., C. Gerbeaud, T. Pott, L. Fernandez-Puente, I. Bivas, M. D. Mitov, J. Dufourcq, and P. Bothorel, 1997. Bending elasticities of model mem-

- branes: influences of temperature and sterol content. *Biophys. J.* 72:2616–2629.
23. Lyatskaya, Y., Y. Liu, S. Tristram-Nagle, J. Katsaras, and J. F. Nagle, 2000. Method for obtaining structure and interactions from oriented lipid bilayers. *Phys. Rev. E* 63:011907.
  24. Evans, E., and W. Rawicz, 1990. Entropy-driven tension and bending elasticity in condensed-fluid membranes. *Phys. Rev. Lett.* 64:2094–2097.
  25. Boulgaropoulos, B., M. Rappolt, B. Sartori, H. Amenitsch, and G. Pabst, 2012. Lipid Sorting by Ceramide and the Consequences for Membrane Proteins. *Biophys. J.* 102:2031–2038.
  26. LeNeveu, D. M., and R. P. Rand, 1977. Measurement and modification of forces between lecithin bilayers. *Biophys. J.* 18:209–230.
  27. Parsegian, V. A., N. Fuller, and R. P. Rand, 1979. Measured work of deformation and repulsion of lecithin bilayers. *PNAS* 76:2750–2754.
  28. Parsegian, V. A., R. P. Rand, N. L. Fuller, and D. C. Rau, 1986. Osmotic stress for the direct measurement of intermolecular forces. In Lester Packer, editor, *Methods in Enzymology*, Academic Press, volume 127 of *Biomembranes Part O: Protons and Water: Structure and Translocation*, 400–416.
  29. McIntosh, T. J., and S. A. Simon, 1986. Hydration force and bilayer deformation: a reevaluation. *Biochemistry* 25:4058–4066.

30. McIntosh, T. J., and S. A. Simon, 1993. Contributions of hydration and steric (entropic) pressures to the interactions between phosphatidylcholine bilayers: Experiments with the subgel phase. *Biochemistry* 32:8374–8384.
31. Rand, R. P., and V. A. Parsegian, 1989. Hydration Forces Between Phospholipid Bilayers. *Biochim. Biophys. Acta* 988:351–376.
32. Petrache, H. I., N. Goulianev, S. Tristram-Nagle, R. Zhang, R. M. Suter, and J. F. Nagle, 1998. Interbilayer interactions from high-resolution x-ray scattering. *Phys. Rev. E* 57:7014–7024.
33. Pabst, G., S. Danner, R. Podgornik, and J. Katsaras, 2007. Entropy-Driven Softening of Fluid Lipid Bilayers by Alamethicin. *Langmuir* 23:11705–11711.
34. Pabst, G., N. Kučerka, M.-P. Nieh, M. C. Rheinstädter, and J. Katsaras, 2010. Applications of neutron and X-ray scattering to the study of biologically relevant model membranes. *Chem. Phys. Lipids* 163:460–479.
35. Sornette, D., and N. Ostrowsky, 1986. Importance of membrane fluidity on bilayer interactions. *J. Chem. Phys.* 84:4062–4067.
36. Evans, E. A., and V. A. Parsegian, 1986. Thermal-mechanical fluctuations enhance repulsion between bimolecular layers. *PNAS* 83:7132–7136.
37. Mecke, K. R., T. Charitat, and F. Graner, 2003. Fluctuating Lipid Bilayer in an Arbitrary Potential: Theory and Experimental Determination of Bending Rigidity. *Langmuir* 19:2080–2087.

38. Gouliaev, N., and J. F. Nagle, 1998. Simulations of Interacting Membranes in the Soft Confinement Regime. *Phys. Rev. Lett.* 81:2610–2613.
39. Gouliaev, N., and J. F. Nagle, 1998. Simulations of a single membrane between two walls using a Monte Carlo method. *Phys. Rev. E* 58:881–888.
40. Zhao, J., J. Wu, F. A. Heberle, T. T. Mills, P. Klawitter, G. Huang, G. Costanza, and G. W. Feigenson, 2007. Phase studies of model biomembranes: Complex behavior of DSPC/DOPC/Cholesterol. *Biochim. Biophys. Acta, Biomembr.* 1768:2764–2776.
41. Heberle, F. A., J. Wu, S. L. Goh, R. S. Petruzielo, and G. W. Feigenson, 2010. Comparison of Three Ternary Lipid Bilayer Mixtures: FRET and ESR Reveal Nanodomains. *Biophys. J.* 99:3309–3318.
42. Heberle, F. A., R. S. Petruzielo, J. Pan, P. Drazba, N. Kučerka, R. F. Standardaert, G. W. Feigenson, and J. Katsaras, 2013. Bilayer Thickness Mismatch Controls Domain Size in Model Membranes. *J. Am. Chem. Soc.* 135:6853–6859.
43. Supplier provided  $M_W$ , accounting for an additional water molecule with DOPC, were used for determining stock concentrations.
44. Cohen, J. A., R. Podgornik, P. L. Hansen, and V. A. Parsegian, 2009. A Phenomenological One-Parameter Equation of State for Osmotic Pressures of PEG and Other Neutral Flexible Polymers in Good Solvents†. *J. Phys. Chem. B* 113:3709–3714.



45. Stanley, C. B., and H. H. Strey, 2003. Measuring Osmotic Pressure of Poly(ethylene glycol) Solutions by Sedimentation Equilibrium Ultracentrifugation. *Macromolecules* 36:6888–6893.
46. Amenitsch, H., M. Rappolt, M. Kriechbaum, H. Mio, P. Laggner, and S. Bernstorff, 1998. First performance assessment of the small-angle X-ray scattering beamline at ELETTRA. *J. Synchrotron Radiat.* 5:506–508.
47. Bernstorff, S., H. Amenitsch, and P. Laggner, 1998. High-Throughput Asymmetric Double-Crystal Monochromator of the SAXS Beamline at ELETTRA. *J. Synchrotron Radiat.* 5:1215–1221.
48. Huang, T. C., H. Toraya, T. N. Blanton, and Y. Wu, 1993. X-ray powder diffraction analysis of silver behenate, a possible low-angle diffraction standard. *J. Appl. Crystallogr.* 26:180–184.
49. Hammersley, A. P., 1997. FIT2D: an introduction and overview. *European Synchrotron Radiation Facility Internal Report ESRF97HA02T* .
50. Hammersley, A. P., S. O. Svensson, M. Hanfland, A. N. Fitch, and D. Hausermann, 1996. Two-dimensional detector software: From real detector to idealised image or two-theta scan. *High Pressure Res.* 14:235–248.
51. Konarev, P. V., V. V. Volkov, A. V. Sokolova, M. H. J. Koch, and D. I. Svergun, 2003. PRIMUS: a Windows PC-based system for small-angle scattering data analysis. *J. Appl. Crystallogr.* 36:1277–1282.
52. Ref. 11. We checked the X-ray analysis for coexisting phases by comparing it with PEG-free, homogeneous samples prepared at the published tie-line

endpoint concentrations of (0.79:0.09:0.12) for Ld and (0.05:0.65:0.30) for the Lo phase (41). These samples were also helpful for constraining some model details (the widths and distances between molecular subgroups composing the lipid heads) in the X-ray analysis.

53. Zhang, R., R. M. Suter, and J. F. Nagle, 1994. Theory of the structure factor of lipid bilayers. *Phys. Rev. E* 50:5047–5060.
54. Caillé, A., 1972. Physique cristalline: remarques sur la diffusion des rayons X dans les smectiques. *C. R. Acad. Sc. Paris Sie B.* 274:891–893.
55. Kučerka, N., J. F. Nagle, J. N. Sachs, S. E. Feller, J. Pencer, A. Jackson, and J. Katsaras, 2008. Lipid Bilayer Structure Determined by the Simultaneous Analysis of Neutron and X-Ray Scattering Data. *Biophys. J.* 95:2356–2367.
56. Rawicz, W., B. Smith, T. McIntosh, S. Simon, and E. Evans, 2008. Elasticity, Strength, and Water Permeability of Bilayers that Contain Raft Microdomain-Forming Lipids. *Biophys. J.* 94:4725–4736.
57. Rawicz, W., K. C. Olbrich, T. McIntosh, D. Needham, and E. Evans, 2000. Effect of Chain Length and Unsaturation on Elasticity of Lipid Bilayers. *Biophys. J.* 79:328–339.
58. Gouliaev, N., 1998. Monte-Carlo simulations of membrane systems. Ph.D. thesis, Carnegie Mellon University, Pittsburgh, Pennsylvania, USA.
59. Specifically, we use  $d_B = 2(z_{CholCH3} + \sigma_{CholCH3})$ , where  $z_{CholCH3}$  and  $\sigma_{CholCH3}$  are the position (measured from the bilayer center) and the width,

respectively, of the lipid head choline's  $\text{CH}_3$  groups. Within measurement accuracy, the definition used in Ref. 32 yields equal values.

60. McDonald, I., 1972. NpT-ensemble Monte Carlo calculations for binary liquid mixtures. *Mol. Phys.* 23:41–58.
61. Bouzida, D., S. Kumar, and R. H. Swendsen, 1992. Efficient Monte Carlo methods for the computer simulation of biological molecules. *Phys. Rev. A* 45:8894–8901.
62. Cooke, I. R., and M. Deserno, 2005. Solvent-free model for self-assembling fluid bilayer membranes: Stabilization of the fluid phase based on broad attractive tail potentials. *J. Chem. Phys.* 123:224710.
63. Pabst, G., N. Kučerka, M.-P. Nieh, and J. Katsaras, 2014. Liposomes, Lipid Bilayers and Model Membranes: From Basic Research to Application. CRC Press.
64. An additional steric repulsion  $A_{st}\lambda_{st}\exp(-a/\lambda_{st})$ , with  $A_{st} = 3.6$  GPa and  $\lambda_{st} = 0.6$  Å according to (71) was used, but proved unimportant for realistic parameters.
65. Marčelja, S., and N. Radić, 1976. Repulsion of interfaces due to boundary water. *Chem. Phys. Lett.* 42:129–130.
66. Kanduč, M., E. Schneck, and R. R. Netz, 2013. Hydration interaction between phospholipid membranes: insight into different measurement ensembles from atomistic molecular dynamics simulations. *Langmuir* 29:9126–9137.

67. Kanduč, M., A. Schlaich, E. Schneck, and R. R. Netz, 2014. Hydration repulsion between membranes and polar surfaces: Simulation approaches versus continuum theories. *Adv. Colloid Interface Sci.* 208:142–152.
68. Parsegian, V. A., 2006. Van der Waals forces. Cambridge university press Cambridge etc.
69. The van der Waals potential for infinitely extended slabs of finite thickness  $d_B$  at separation  $a$  is  $\propto (1/a^2 - 2/(a + d_B)^2 + 1/(a + 2d_B)^2)$  (68, p. 15), and was applied for osmotic stress experiments in e.g. Refs 8, 32.
70. Podgornik, R., R. H. French, and V. A. Parsegian, 2006. Nonadditivity in van der Waals interactions within multilayers. *J. Chem. Phys.* 124:044709.
71. McIntosh, T. J., A. D. Magid, and S. A. Simon, 1987. Steric repulsion between phosphatidylcholine bilayers. *Biochemistry* 26:7325–7332.
72. Although this model gives only a first order estimate for the van der Waals interactions of fluctuating lipid bilayers, it is to our knowledge the best available approximation in the absence of data on the dielectric response of PC lipids. Further effects of, e.g. lipid headgroup dipolar moment fluctuations (89), could be considered as well, but they would be only important at very small separations where hydration forces dominate and the exact form of the van der Waals interaction is irrelevant.
73. Equation (4) was derived from  $P_j(d_W) \approx -\partial\Phi_j(d_W)/\partial d_W$ . The difference to the exact relationship  $P_j(d_W) = \langle -\partial\Phi(\bar{a})/\partial\bar{a} \rangle$  was found to be less than the simulational uncertainty.

74. 2011. MATLAB v. 7.12 (R2011a).
75. Taylor, J., 1997. Introduction to Error Analysis, the Study of Uncertainties in Physical Measurements, 2nd Edition, volume 1. University Science Books, New York.
76. Alternatively, one could have used optimization algorithms specialized for simulations (90–93), but the existing implementations did not satisfy our needs.
77. Hemmerle, A., L. Malaquin, T. Charitat, S. Lecuyer, G. Fragneto, and J. Daillant, 2012. Controlling interactions in supported bilayers from weak electrostatic repulsion to high osmotic pressure. *PNAS* 109:19938–19942.
78. Pabst, G., 2006. Global properties of biomimetic membranes: perspectives on molecular features. *Biophys. Rev. Lett.* 01:57–84.
79. The small offset  $\delta = 200$  Pa is necessary for plotting  $P = 0$  on a logarithmic scale.
80. Pan, J., T. T. Mills, S. Tristram-Nagle, and J. F. Nagle, 2008. Cholesterol Perturbs Lipid Bilayers Nonuniversally. *Phys. Rev. Lett.* 100:198103.
81. Sorre, B., A. Callan-Jones, J.-B. Manneville, P. Nassoy, J.-F. Joanny, J. Prost, B. Goud, and P. Bassereau, 2009. Curvature-driven lipid sorting needs proximity to a demixing point and is aided by proteins. *PNAS* 106:5622–5626.

82. Tian, A., B. R. Capraro, C. Esposito, and T. Baumgart, 2009. Bending Stiffness Depends on Curvature of Ternary Lipid Mixture Tubular Membranes. *Biophys. J.* 97:1636–1646.
83. Gracià, R. S., N. Bezlyepkina, R. L. Knorr, R. Lipowsky, and R. Dimova, 2010. Effect of cholesterol on the rigidity of saturated and unsaturated membranes: fluctuation and electrodeformation analysis of giant vesicles. *Soft Matter* 6:1472–1482.
84. Khelashvili, G., B. Kollmitzer, P. Heftberger, G. Pabst, and D. Harries, 2013. Calculating the Bending Modulus for Multicomponent Lipid Membranes in Different Thermodynamic Phases. *J. Chem. Theory Comput.* 9:3866–3871.
85. Pan, J., S. Tristram-Nagle, and J. F. Nagle, 2009. Effect of cholesterol on structural and mechanical properties of membranes depends on lipid chain saturation. *Phys. Rev. E* 80:021931.
86. This relation was suggested by Evan Evans (85).
87. Veatch, S. L., and S. L. Keller, 2003. Separation of Liquid Phases in Giant Vesicles of Ternary Mixtures of Phospholipids and Cholesterol. *Biophys. J.* 85:3074–3083.
88. Scherfeld, D., N. Kahya, and P. Schwille, 2003. Lipid Dynamics and Domain Formation in Model Membranes Composed of Ternary Mixtures of Unsaturated and Saturated Phosphatidylcholines and Cholesterol. *Biophys. J.* 85:3758–3768.

89. Podgornik, R., 1988. Solvent structure effects in dipole correlation forces. *Chem. Phys. Lett.* 144:503–508.
90. Ben-Tal, A., and A. Nemirovski, 1999. Robust solutions of uncertain linear programs. *Operations Research Letters* 25:1–13.
91. Ben-Tal, A., and A. Nemirovski, 2000. Robust solutions of Linear Programming problems contaminated with uncertain data. *Math. Program.* 88:411–424.
92. Fu, M. C., 2002. Feature Article: Optimization for simulation: Theory vs. Practice. *INFORMS Journal on Computing* 14:192–215.
93. Ben-Tal, A., A. Goryashko, E. Guslitzer, and A. Nemirovski, 2004. Adjustable robust solutions of uncertain linear programs. *Math. Program., Ser. A* 99:351–376.
94. Salsburg, Z. W., J. D. Jacobson, W. Fickett, and W. W. Wood, 1959. Application of the Monte Carlo Method to the Lattice-Gas Model. I. Two-Dimensional Triangular Lattice. *J. Chem. Phys.* 30:65–72.
95. Ferrenberg, A. M., and R. H. Swendsen, 1988. New Monte Carlo technique for studying phase transitions. *Phys. Rev. Lett.* 61:2635–2638.
96. Ferrenberg, A. M., and R. H. Swendsen, 1989. Optimized Monte Carlo data analysis. *Phys. Rev. Lett.* 63:1195–1198.
97. Kumar, S., J. M. Rosenberg, D. Bouzida, R. H. Swendsen, and P. A. Kollman,

1992. The weighted histogram analysis method for free-energy calculations on biomolecules. I. The method. *J. Comput. Chem.* 13:1011–1021.
98. Nagle, J. F., 2013. Introductory Lecture: Basic quantities in model biomembranes. *Faraday Discuss.* 161:11.
99. Chu, N., N. Kučerka, Y. Liu, S. Tristram-Nagle, and J. F. Nagle, 2005. Anomalous swelling of lipid bilayer stacks is caused by softening of the bending modulus. *Phys. Rev. E* 71:041904.
100. Bonner, J. C., and M. E. Fisher, 1964. Linear Magnetic Chains with Anisotropic Coupling. *Phys. Rev.* 135:A640–A658.
101. Nagle, J. F., and J. C. Bonner, 1970. Numerical studies of the Ising chain with long-range ferromagnetic interactions. *J. Phys. C: Solid State Phys.* 3:352.
102. Quenouille, M. H., 1956. Notes on Bias in Estimation. *Biometrika* 43:353–360.
103. Tukey, J. W., 1958. Bias and confidence in not quite large samples (abstract). *Ann. Math. Statist.* 29:614.



# Supporting information for: Bending rigidities and interdomain forces in membranes with coexisting lipid domains

B. Kollmitzer, P. Heftberger, R. Podgornik,  
J. F. Nagle, and G. Pabst

April 15, 2015, Graz

## S1 Area extension modulus estimation

The dependence of bilayer thickness on osmotic pressure  $P$  is accounted for via the area extension modulus  $K_A$  and given by the equation<sup>1</sup>

$$d_B(P) = d_B(0) \frac{K_A + P d(P)}{K_A + P d_B(0)}. \quad (\text{S1})$$

We estimated  $K_A$  for our coexisting liquid phases based on published data for single lipids and binary lipid mixtures by Rawicz *et al.*<sup>2,3</sup> The Ld phase under investigation consists essentially of DOPC, with approximately 10 mol% cholesterol.<sup>4</sup> Interpolating linearly between the two published values for 0 and 50 mol% cholesterol in DOPC<sup>2</sup> yields  $K_A(\text{Ld}) = (430 \pm 30) \text{ mN m}^{-1}$ .

In the coexisting Lo phase, the main constituent is the saturated lipid DSPC, which is accompanied by ca. 30 mol% cholesterol.<sup>4</sup> Unfortunately, published  $K_A$  values for saturated lipids are sparse. As a compromise, we interpolated linearly between pure DMPC (0 mol% cholesterol) and a 1:1 mixture of sphingomyelin/cholesterol,<sup>2,3</sup> yielding  $K_A = (2100 \pm 500) \text{ mN m}^{-1}$  for our Lo phase.

As pointed out in the section *X-ray measurements* of the main text, knowing the magnitude of  $K_A$  is more important than getting the precise number. That is because the biggest estimated change in bilayer thickness turned out to be just 0.3 Å. In principle, such a subtle difference in  $d_B$  would be resolvable with SAXS, but not with the additional scattering signal due to PEG.

## S2 Finite size convergence

With open edges, one generally expects a ‘surface’ perturbation proportional to the relative size of the boundary to the interior, i.e. proportional to  $1/N$  for our systems. As is

well known, periodic boundary conditions generally reduce this perturbation. They also speed up the convergence with system size, from  $1/N$  to  $1/N^2$  in a case well documented by Bonner and Fisher<sup>5</sup> (note their Fig. 1) and in the case of the one-dimensional Ising model the convergence is exponentially fast with periodic boundary conditions. While another case with very slow convergence is known,<sup>6</sup> that one is due to very long range interactions not present in our membrane stacks. For periodic boundary conditions, the exact solution of a harmonic approximation to Eq. (3) suggests that  $d_W$  and  $\Delta$  converge asymptotically like  $y(N) \sim c_\infty - c_2/N^2$ , i.e. convergence is expected to be faster than  $1/N$  and, in agreement with the previous simulations,<sup>7</sup> our results are consistent with a dominant  $1/N^2$  asymptotic convergence, allowing, of course, for higher order terms.

We perform simulations for several ‘densities’  $N \in \{N_{min}, \dots, N_{max}\}$  and fit them with the function  $y(N) = c_\infty + \sum_{k=2}^{k_{max}} c_k/N^k$ . Together with the originally proposed  $k_{max} = 3$  and  $N \in \{6, \dots, 32\}$ , this method yields sufficiently precise continuum estimators  $c_\infty$ , compared to the experimental uncertainties.<sup>8</sup> However, we found that varying the arbitrary parameters  $k_{max}$  and  $N_{min}$  influenced the final estimator stronger for some simulations (e.g. high pressures) than for others. To obtain more reliable uncertainties and perhaps even better continuum estimates, we perform now several extrapolations, with different values for  $k_{max}$  and  $N_{min}$ , but always using the highest possible  $N_{max}$ . By not changing  $N_{max}$ , we weight the most significant simulations (with the highest density) stronger. This procedure yields a list of results for  $c_{\infty,l}$ , which we average for the final estimator. Its uncertainty is then determined by the individual errors of  $c_{\infty,l}$  (statistical uncertainty of observables due to finite simulation length) and their standard deviation (error due to finite simulation density). This procedure is closely related to the Jackknife technique.<sup>9,10</sup>

Comparisons between these improved Jackknife estimators and estimators obtained by the original method are given in Fig. S1. The relative difference in the estimators were less than 5% for all performed simulations, but most importantly, Jackknife produces a meaningful uncertainty.

### S3 Efficient differentiation

A single simulation of a particular set of parameters  $\vec{\Lambda} = (P, A, H, \lambda, K_c, \dots)$  contains more information in the generated time series, than the aforementioned observables which are determined by averaging. By reweighting the simulated histogram of density of states, it is possible to compute these quantities over a certain range of simulation parameters and thereby also derive their gradients.<sup>11–13,14</sup> This well recognized method was briefly mentioned for membrane MC simulations,<sup>15</sup> but has not been implemented for them previously.

We calculated the expectation value of an observable  $f(u, \bar{a})$  for a different set of parameters  $\vec{\Lambda}'$  from a simulation performed at  $\vec{\Lambda}$  by

$$\langle f \rangle_{\vec{\Lambda}'} = \frac{\sum f_{\vec{\Lambda}'}(u, \bar{a}) \cdot \exp(-\delta G/kT)}{\sum \exp(-\delta G/kT)}, \quad (\text{S2})$$

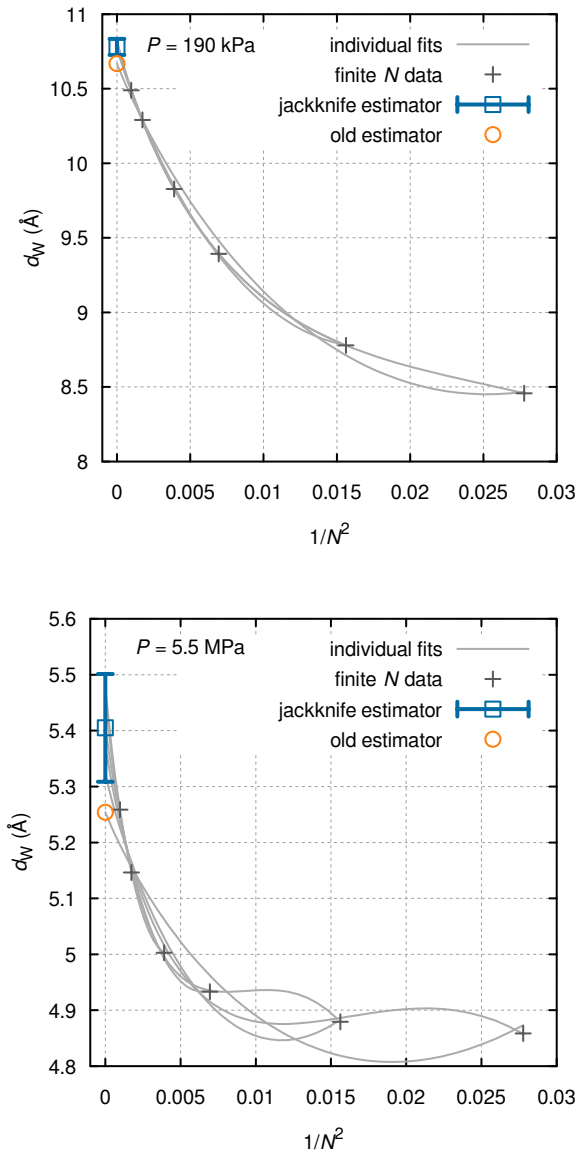


Figure S1: Finite size convergence of membrane spacing  $d_W$  vs membrane “density”  $N$  of Ld domains according to Tab. 1 at intermediate (top) and high osmotic pressures  $P$  (bottom). A variant of Jackknife allows us to obtain reasonable errors for the estimator. Statistical uncertainties for plotted finite  $N$  data are less than  $10^{-2}$  Å.

where the sums extend over all realized configurations and  $\delta G$  is the change in the Gibbs energy of each state  $(u, \bar{a})$  upon changing  $\vec{\Lambda}$  to  $\vec{\Lambda}'$ . Most parameters could be separated from  $u$  and  $\bar{a}$  in our case, yielding  $\delta G(u, \bar{a}) = \delta \Lambda \cdot \xi(u, \bar{a})$ . This allowed us to store only the time series of  $\xi$  instead of all realized states. The parameters  $P$ ,  $A$ ,  $H$ , and  $K_c$  were separable in this way, yielding

$$\frac{\delta G}{V} = \delta P \xi_P + \delta A \lambda \xi_A - \frac{\delta H}{12\pi} \xi_H + N^2 \frac{\delta K_c}{2} \xi_{K_c}, \quad (\text{S3})$$

where  $\xi_P = \bar{a}/d_W$ ,  $\xi_A = \overline{\exp(-a/\lambda)}$ ,  $\xi_H = \overline{1/a^2}$ , and  $\xi_{K_c} = \overline{q^4 |u_m(q_x, q_y)|^2}$ . The local distance between membranes is denoted by  $a = u_{m+1}(x, y) - u_m(x, y) + \bar{a}$ , while the bars denote averages over  $(m, x, y)$  or  $(m, q_x, q_y)$ .  $V = L^2 M \bar{a}$  is the membrane stack's volume.

Separating  $\lambda$  from  $(u, \bar{a})$  in  $\delta G$  turned out to be impossible, but we were able to calculate gradients of  $d_W$  and  $\Delta$  with respect to  $\lambda$  efficiently. Because  $d_W$  and  $\Delta$  did not depend explicitly on  $\lambda$  (i.e.  $\partial f/\partial \lambda = 0$ ), differentiating Eq. (S2) yielded,

$$\left. \frac{\partial \langle f \rangle_{\lambda'}}{\partial \lambda'} \right|_{\lambda'=\lambda} = -\frac{AV}{kTN^2\Omega} \left( \sum f(u, \bar{a}) \xi_\lambda - \langle f \rangle_\lambda \sum \xi_\lambda \right), \quad (\text{S4})$$

where sums extend over all realized states,  $\Omega$  denotes the collection length and

$$\xi_\lambda = \overline{\left( 1 + \frac{a}{\lambda} \right) \exp\left( -\frac{a}{\lambda} \right)}. \quad (\text{S5})$$

Up to first order,  $\langle f \rangle_{\lambda'}$  was then determined from  $\langle f \rangle_{\lambda'} \approx \langle f \rangle_\lambda + (\lambda' - \lambda) \partial \langle f \rangle / \partial \lambda$ .

Thus, for any observable  $f \in \{d_W, \Delta\}$  and parameter  $\Lambda \in \{P, A, H, K_c, \lambda\}$ , we first determined  $\langle f \rangle_{1,2}(N)$  for  $\Lambda_{1,2} = \Lambda \pm \delta \Lambda$  as detailed above, extrapolated these expectation values for  $N \rightarrow \infty$  according to section S2, and finally calculated the finite difference quotient  $\partial \langle f \rangle / \partial \Lambda \approx (\langle f \rangle_1 - \langle f \rangle_2) / 2\delta \Lambda$ . Relative finite differences were set to  $\delta \Lambda / \Lambda = 0.03$ .

We checked this method against direct numerical differentiation for a couple of reasonable parameters. Errors were always sufficiently small (well below 50%) to lead the optimization routine towards a global minimum (see the section *Optimizing parameters against experimental data* of the main text).

## S4 Results for a homogeneous control sample

We tested our analysis on already published SAXS data for homogeneous DMPC MLVs determined at 30 °C.<sup>16</sup> The Lifshitz calculation of the van der Waals forces yielded a value of  $H = 4.11$  zJ for the published bilayer thickness of 44.0 Å. The obtained values describing the intersurface forces are given in Tab. S1, while Fig. S2 compares the simulations with the experimental data. Reassuringly, the simulations fit the experimental osmotic pressure data well. While the fit to  $\Delta$  is excellent for high hydration, the fit becomes relatively poor for  $\Delta$  as  $d_W$  becomes small, similarly to our  $L_o$  sample and likely for the same reason given in the main text.

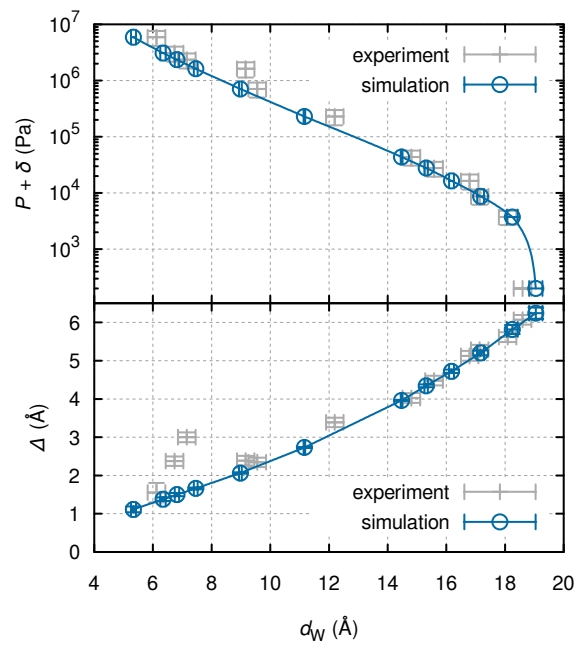


Figure S2: Osmotic pressure (top) and fluctuations (bottom) vs water-layer thickness for best fit of membrane MC simulation (cyan) against SAXS data (light gray) obtained from Ref. 16.<sup>17</sup> Solid lines were obtained by exponentially interpolating fluctuation contributions.

The interaction parameters obtained from the fit are shown in Tab. S1. Literature values for DMPC’s bending modulus range from 50–130 zJ at 30 °C.<sup>18</sup> In light of this large variation, comparing only results of related methods is appropriate. Ref. 16 could not determine  $K_c$  and the modulus  $B$  separately and therefore considered several values of  $K_c$ ; two of these are shown in Tab. S1. The values of  $A$  agree very well with ours. The larger values of  $\lambda$  would have been smaller if the true value of  $K_A$  had been known at that time. Two differences from the previous analyses are that here we calculated  $H$  and we used simulations; these cause the main differences reflected in the pairs of values for  $H$  and  $K_c$  in Tab. S1. Table S1 also shows results from another study,<sup>19</sup> that employed the same kind of simulations used here and differed by obtaining X-ray data from oriented stacks of DMPC bilayers, from which  $K_c$  was obtained directly. It also used the same  $P$  data, but failed to readjust the  $A$  and  $\lambda$  values to account for the corrected  $K_A$ . Nevertheless, agreement is reasonable.

Table S1: Optimal parameters found for describing the DMPC data published in Ref. 16.

	Current	1998a <sup>16</sup>	1998b <sup>16</sup>	2005 <sup>19</sup>
$H/\text{zJ}$	4.11	7.13	4.91	6.1
$K_c/\text{zJ}$	$57 \pm 5$	50	80	69
$A/\text{Pa}$	$10^{8.1 \pm 0.2}$	$10^{8.1}$	$10^{8.1}$	$10^{8.1}$
$\lambda/\text{\AA}$	$1.66 \pm 0.15$	1.91	1.97	1.91

For completeness, the functional dependence of the individual fundamental surface forces for DMPC is plotted in Fig. S3. The fluctuation force becomes the dominant repulsive force when  $d_W$  exceeds 9 Å, intermediate between the values of the Ld and Lo phases in Fig. 7, suggesting that the DMPC bilayer fluctuations are intermediate in this regard between the more fluid Ld phase and the more ordered Lo phase in the studied mixture. This is consistent with the Ld phase having a high concentration of the more disordered unsaturated lipids and the Lo phase having longer saturated chains with cholesterol.

## S5 SAXS analysis

Comparisons between full  $q$ -range SAXS analyses and experimental data are shown in Fig. S4. Deviations between data and fits, especially for higher  $q$  ranges, are due to imperfect background subtraction, as explained in the section *X-ray measurements* in the main text.

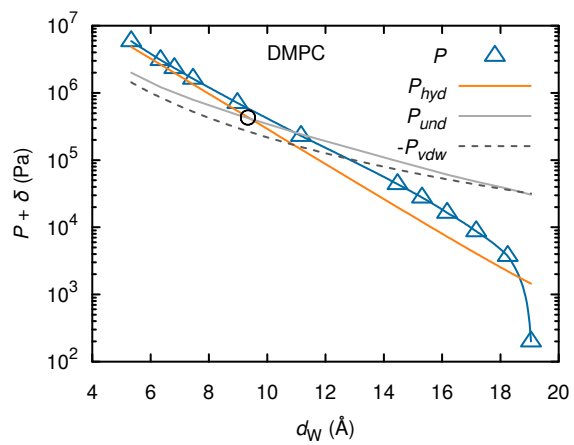


Figure S3: Partitioning of total pressure  $P$  into contributions from hydration  $P_{hyd}$ , van der Waals  $P_{vdw}$ , and undulations  $P_{und}$  for DMPC.<sup>17</sup> The large open black circle shows the value of the separation  $d_W$  at which hydration and undulation pressure are equal.

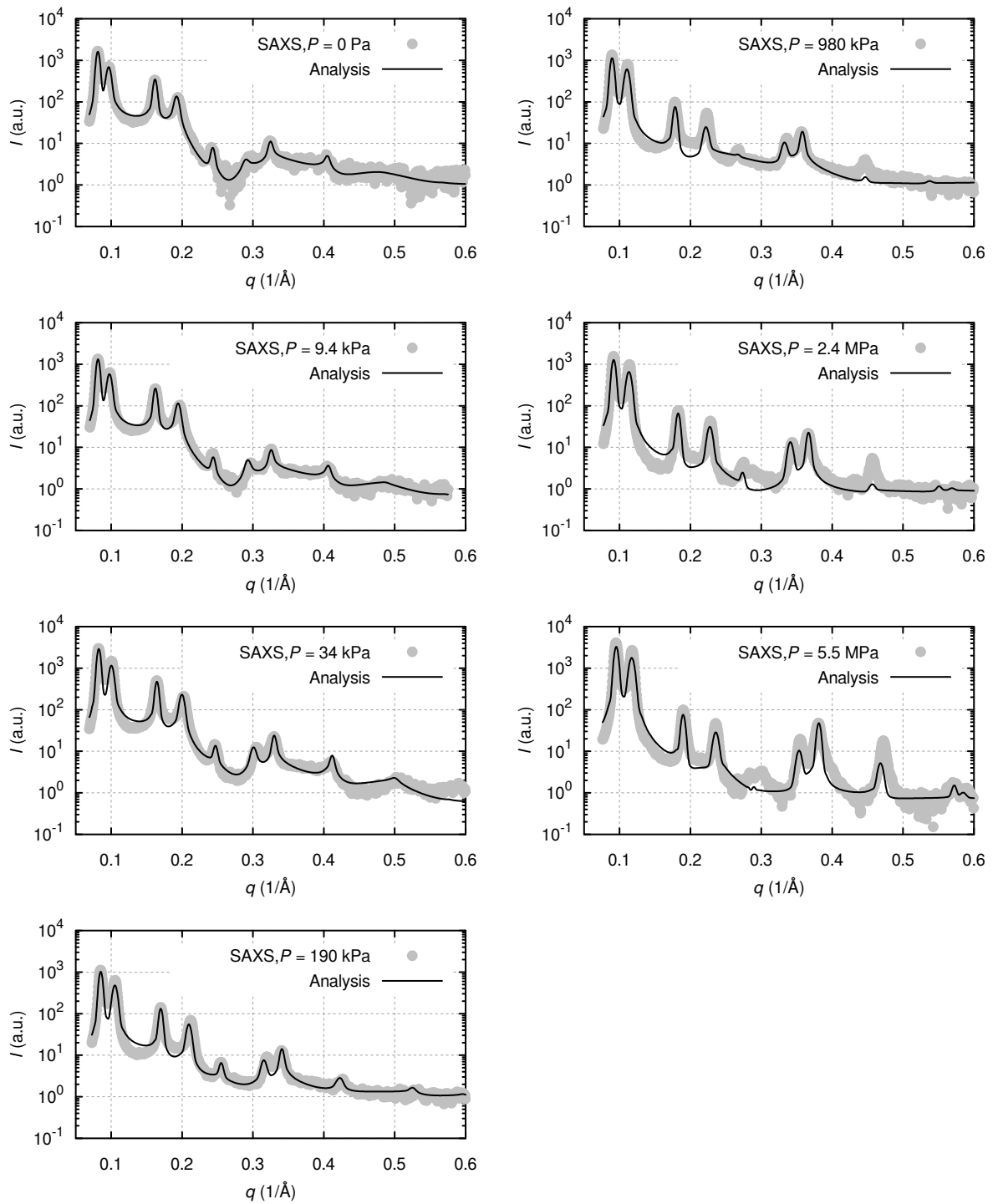


Figure S4: Calculated scattering intensities (solid lines) from full  $q$ -range analyses, compared to recorded SAXS data from coexisting phases (dots) of DOPC/DSPC/Chol (0.42:0.37:0.21), for all recorded osmotic pressures  $P$ .



## S6 Fluctuations of the interbilayer water spacing

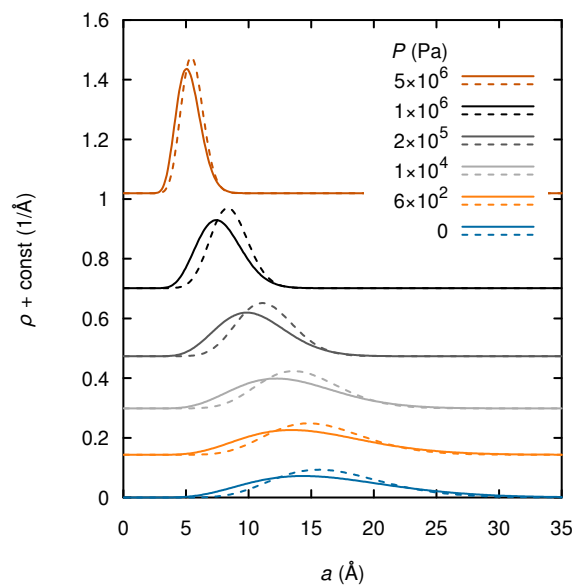


Figure S5: Probability density function  $\rho$  of the water spacing  $a$  at different external pressures  $P$ , for Ld (solid) and Lo (dashed) according to Tab. 1, obtained from  $N = 32$  simulations.

## References

- [1] R. P. Rand and V. A. Parsegian. Hydration Forces Between Phospholipid-Bilayers. *Biochim. Biophys. Acta*, 988(3):351–376, December 1989.
- [2] W. Rawicz, B.A. Smith, T.J. McIntosh, S.A. Simon, and E. Evans. Elasticity, Strength, and Water Permeability of Bilayers that Contain Raft Microdomain-Forming Lipids. *Biophys. J.*, 94(12):4725–4736, June 2008.
- [3] W. Rawicz, K. C. Olbrich, T. McIntosh, D. Needham, and E. Evans. Effect of Chain Length and Unsaturation on Elasticity of Lipid Bilayers. *Biophys. J.*, 79(1):328–339, July 2000.
- [4] Frederick A. Heberle, Jing Wu, Shih Lin Goh, Robin S. Petruzielo, and Gerald W. Feigenson. Comparison of Three Ternary Lipid Bilayer Mixtures: FRET and ESR Reveal Nanodomains. *Biophys. J.*, 99(10):3309–3318, November 2010.
- [5] Jill C. Bonner and Michael E. Fisher. Linear Magnetic Chains with Anisotropic Coupling. *Phys. Rev.*, 135(3A):A640–A658, August 1964.
- [6] J. F. Nagle and J. C. Bonner. Numerical studies of the Ising chain with long-range ferromagnetic interactions. *J. Phys. C: Solid State Phys.*, 3(2):352, February 1970.
- [7] Nikolai Gouliarov and John F. Nagle. Simulations of Interacting Membranes in the Soft Confinement Regime. *Phys. Rev. Lett.*, 81(12):2610–2613, September 1998.
- [8] Nikolai Gouliarov and John F. Nagle. Simulations of a single membrane between two walls using a Monte Carlo method. *Phys. Rev. E*, 58(1):881–888, July 1998.
- [9] M. H. Quenouille. Notes on Bias in Estimation. *Biometrika*, 43(3/4):353–360, December 1956.
- [10] John W. Tukey. Bias and confidence in not quite large samples (abstract). *Ann. Math. Statist.*, 29(2):614, June 1958.
- [11] Z. W. Salsburg, J. D. Jacobson, W. Fickett, and W. W. Wood. Application of the Monte Carlo Method to the Lattice-Gas Model. I. Two-Dimensional Triangular Lattice. *J. Chem. Phys.*, 30(1):65–72, January 1959.
- [12] Alan M. Ferrenberg and Robert H. Swendsen. New Monte Carlo technique for studying phase transitions. *Phys. Rev. Lett.*, 61(23):2635–2638, December 1988.
- [13] Alan M. Ferrenberg and Robert H. Swendsen. Optimized Monte Carlo data analysis. *Phys. Rev. Lett.*, 63(12):1195–1198, September 1989.
- [14] A common extension of this method would even allow to combine information from multiple simulations (WHAM)<sup>20</sup>.

- [15] Nikolai Gouliaev. *Monte-Carlo simulations of membrane systems*. PhD thesis, Carnegie Mellon University, Pittsburgh, Pennsylvania, USA, July 1998.
- [16] Horia I. Petrache, Nikolai Gouliaev, Stephanie Tristram-Nagle, Ruitian Zhang, Robert M. Suter, and John F. Nagle. Interbilayer interactions from high-resolution x-ray scattering. *Phys. Rev. E*, 57(6):7014–7024, June 1998.
- [17] The small offset  $\delta = 200$  Pa is necessary for plotting  $P = 0$ .
- [18] John F. Nagle. Introductory Lecture: Basic quantities in model biomembranes. *Faraday Discuss.*, 161:11, 2013.
- [19] Nanjun Chu, Norbert Kučerka, Yufeng Liu, Stephanie Tristram-Nagle, and John F. Nagle. Anomalous swelling of lipid bilayer stacks is caused by softening of the bending modulus. *Phys. Rev. E*, 71(4):041904, April 2005.
- [20] Shankar Kumar, John M. Rosenberg, Djamal Bouzida, Robert H. Swendsen, and Peter A. Kollman. The weighted histogram analysis method for free-energy calculations on biomolecules. I. The method. *J. Comput. Chem.*, 13(8):1011–1021, 1992.